DETERMINATION OF THE INPUT POWER TO A RADIO FREQUENCY ELECTRODELESS DISCHARGE.

BY

WILLIAM LEE WALKER

February 19, 1970

To the Graduate Council:

I am submitting herewith a thesis written by William Lee Walker, entitled "Determination of the Input Power to a Radio Frequency Electrodeless Discharge." I recommend that it be accepted for nine quarter hours of credit in partial fulfillment of the requirements for the degree of Master of Science, with a major in Physics.

DETERMINATION OF THE INPUT POWER TO A RADIO FREQUENCY ELECTRODELESS DISCHARGE

A Thesis

Presented to

the Graduate Council of

The University of Tennessee

In Partial Fulfillment

of the Requirements for the Degree

Master of Science

---

by

William Lee Walker

March 1970

ACKNOWLEDGMENTS

The author is especially grateful and will be forever indebted to Mr. J. A. Sprouse of ARO, Inc., Arnold Engineering Development Center, for suggesting this topic of study and for indoctrinating a beginner into radio frequency plasma research. This work would not have been possible without his guidance and helping hand throughout the course of this work and in particular during the preparation of this study. Appreciation is also expressed to Dr. W. K. McGregor, Jr., R. J. Bryson and the technicians of the Rocket Test Facility, Research Branch, ARO, Inc., for their assistance in running the apparatus.

The author wishes to express appreciation to Dr. A. A. Mason of The University of Tennessee Space Institute for his advice in completing this study and for his help in arranging the final manuscript. Also, appreciation is extended to the U. S. Navy and to Dr. R. L. Young, Deputy Director for Educational Programs, The University of Tennessee Space Institute for making this study possible through the Naval Scholarship Program (SECNAVINST 1500.45.)

Last but not least, sincerest appreciation is expressed for the patience and understanding rendered by my wife and family during the course of this study.

The work reported herein was supported by Headquarters AEDC, Arnold Air Force Station, Tennessee within the terms of Contract F40600-69-C-0001 with ARO, Inc. Reproduction to satisfy the needs of the U.S. Government is authorized.

ABSTRACT

The input power of a radio frequency electrodeless discharge operated at 4 MHZ with a radial inflow of argon at one atmosphere of chamber pressure is measured.

It is found that the discharge does not necessarily operate at maximum efficiency; that is, $\sqrt{2}\ a/\delta \neq 2.5$. The plasma radius to skin depth ratio for the radio frequency system reported here was found to be 12.2, instead of the value $\sqrt{2}\ a/\delta = 2.5$, for which maximum operating efficiency is expected.

TABLE OF CONTENTS

LIST OF FIGURES

NOMENCLATURE

a	Plasma radius
B	Magnetic field
B+	DC plate voltage
B_z	Axial component of magnetic field
C_g	Fine tuning capacitor
C_p	Coarse tuning capacitor
D	Electric displacement
E	Electric field
E_ϕ	Azimuthal component of electric field
I_L	Oscillator coil current
I_T	Radio frequency grid current
J	Current density
KV	Kilovolts
L_p	Oscillator inductor
M-1	Meter, DC plate voltage
M-2	Meter, DC grid voltage
M-3	Meter, cathode current
M-4	Meter, coil voltage
M-5	Meter, radio frequency grid current
P	Plasma power
P_o	Normalized power
P_{dc}	DC power
T-1	Radio frequency current transformer distance
δ	Skin depth

σ	Electric conductivity
ρ	Radial distance
ε_o	Electric permittivity
μ_o	Magnetic permeability
ϕ	Azimuthal angle
ω	Frequency

CHAPTER I

INTRODUCTION

The electrodeless discharge transfers by induction radio frequency power to gases contained within the volume of a solenoid which is carrying a radio frequency current. The axially directed magnetic field within the solenoid induces an azimuthal electric field in accordance with Faraday's Law. The azimuthal eddy currents cause ionization and ohmically heat the gas to high temperatures. This process is of interest to those charged with the development of high enthalpy wind tunnels utilized in reentry testing.

One of the earliest works that is now recognized as the fundamental work in the field of electrodeless plasma production was reported by J. J. Thomson and is described by Hollister [1][1] in an excellent historical review of the literature. Thomson developed the transformer model to describe the discharge and attributed the observed phenomena solely to the electric field. However, at this time J. S. Townsend claimed that the electrodeless discharge was magnetic in origin and published his own theory of the electrodeless discharge [1], which

---

[1]Numbers in brackets refer to similarly numbered references in the bibliography.

disagreed with the Thomson theory. McKinnon [1] resolved the controversy by theoretically demonstrating that two kinds of electrodeless discharges exist: One of electric origin and one of magnetic origin. Experimental observations by Babat [2] were interpreted as proof of the presence of both the Thomson electric discharge and the Townsend magnetic discharge in the same discharge simultaneously.

Radio frequency (rf) electrodeless discharges are manifest in many visible forms, and those who have seen these discharges can testify to the various geometrical configurations which they display, for example, diffuse glow, toroidial discharge, cylindrical plasmoid, arcing, and others. However, all the aforementioned discharges have been divided into two major categories:

(1) The discharges in which the elementary conductance currents are not closed but are continued by dielectric currents are termed "E-discharges."

(2) The discharges in which the conductance currents are in the form of closed curves are termed "H-discharges."

No standard terminology has been adopted and the two modes of discharges have been called respectively: Low-power and high-power, glow and arc, low pressure and high pressure, cold and thermal, and capacitive and inductive. In

this study, only the H-discharge (high-power mode) will be of interest.

The electrodeless discharge described herein is a gaseous discharge which occurs in a flowing argon gas within the volume of the work coil. This coil carries an alternating current of 20 to 80 amperes at a frequency of four megahertz. Once the discharge is ignited in the high-power mode, it manifests itself by a bright, luminous, white cylindrical discharge, confined within the volume of the work coil. With little or no gas flow and at pressures less than one atmosphere, the luminous cylinder extends to the wall of the confining quartz tube and no dark interval can be distinguished between the quartz tube wall and the bright zone.

In order to illustrate some of the visible features of an rf discharge, photographs of the discharge at different flow rates, pressure and power levels are shown in Figure 1.

Recent theoretical energy balance studies of power transfer have been made by Keefer [3], Eckert [4], Hollister [1], and Sprouse [5] which predict values for power transfer that are in agreement with similar predictions from the Thomson theory.

Although there has been considerable theoretical work for determining the rf power delivered to the plasma, very few experimental results have been reported in the

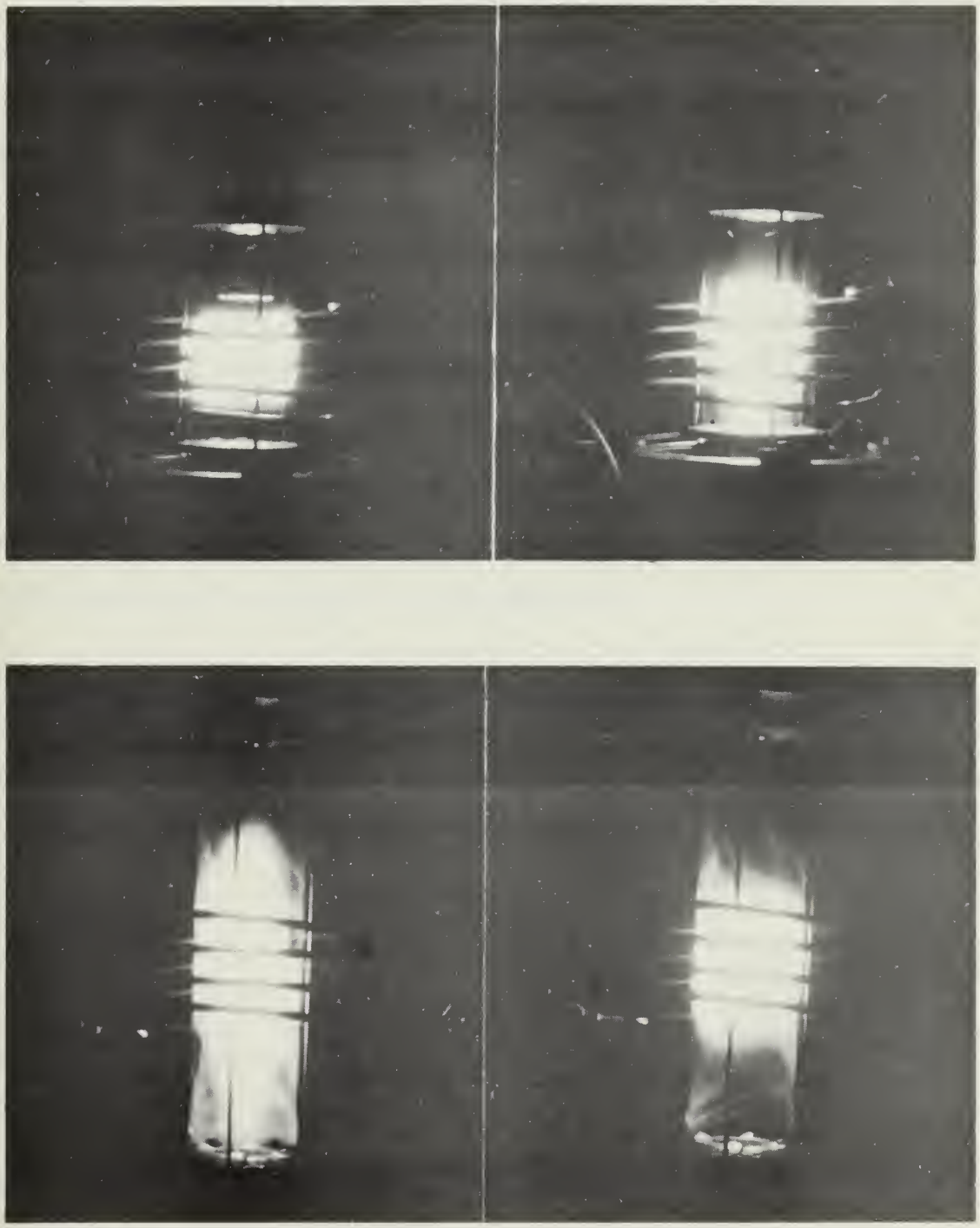

Figure 1. Photographs of the Discharge.

literature. One recent measurement reported is that of Dresvin, Donskoi, and Gol´dfarb [6] who used calorimetric and spectroscopic techniques. The experimental measurement of input power is important to the determination of the rate at which the discharge converts magnetic energy into heat.

It is the purpose of this work to measure the input power to the plasma by two methods. The first method uses the properties of the discharge geometry and the applied magnetic field as predicted in the Thomson model of coupling. The second method measures the current and voltage used to produce the discharge.

CHAPTER II

THEORY

I. THE THOMSON MODEL OF THE ELECTRODELESS DISCHARGE

In this section the Thomson model will be used to develop a mathematical expression relating the plasma power, the input power to the plasma and the magnetic field. The Thomson model assumes the induction solenoid to be long compared to its diameter, thereby neglects end effects. Furthermore, it is assumed that the plasma is uniform and homogeneous and that the variation of the fields is predominantly a function of the radial coordinate, so that the magnetic and electric fields are given by

$$\vec{B} \approx \hat{i}_z \, \text{Real}\{B_z(\rho)e^{i\omega t}\} \tag{1}$$

and

$$\vec{E} \approx \hat{i}_\phi \, \text{Real}\{E_\phi(\rho)e^{i\omega t}\} \tag{2}$$

Maxwell's equation for the fields within the discharge are

$$\nabla \cdot \vec{E} = 0 \tag{3}$$

$$\nabla \cdot \vec{B} = 0 \tag{4}$$

$$\nabla \times \vec{E} = - i\omega\vec{B} \tag{5}$$

$$\nabla \times \vec{B} = \mu_o\vec{J} + i\omega\mu_o\vec{D} \tag{6}$$

The current density $\vec{J}$ is related to the electric field $\vec{E}$ through Ohm's law

$$\vec{J} = \sigma\vec{E} \tag{7}$$

The electric displacement $\vec{D}$ is related to the electric field by

$$\vec{D} = \varepsilon_o\vec{E} \tag{8}$$

Using Equations (7) and (8), Equation (6) becomes

$$\nabla \times \vec{B} = \mu_o\sigma\vec{E} + i\omega\mu_o\varepsilon_o\vec{E} \tag{9}$$

The displacement current within the plasma may be neglected if

$$\sigma >> \omega\varepsilon_o \tag{10}$$

This condition is seen to be satisfied since the electrical conductivity is on the order of 10^3 mhos, ω is of the order of 10^7 sec^{-1} and $\varepsilon_o \sim 10^{-12}$ farads/meter. Maxwell's equations now become

$$\nabla \times \vec{E} = - i\omega\vec{B} \tag{11}$$

$$\nabla \times \vec{B} = \mu_o\sigma\vec{E} \tag{12}$$

When separated into components in cylindrical coordinates (the geometry of the discharge, see Appendix A), we obtain for the curl of $\vec{E}$

$$\nabla \times \vec{E} = \hat{i}_z \left(\frac{\partial E_\phi}{\partial \rho} + \frac{E_\phi}{\rho}\right) = - i\omega \hat{i}_z B_z \tag{13}$$

and recognizing that B_z is the only component of $\vec{B}$ we have

$$\nabla \times \vec{B} = - \hat{i}_\phi \frac{\partial B_z}{\partial \rho} = - \hat{i}_\phi \mu_o \sigma E_\phi \tag{14}$$

From Equation (14), we see that

$$E_\phi = - \frac{1}{\mu_o \sigma} \frac{\partial B_z}{\partial \rho} \tag{15}$$

likewise

$$\frac{\partial E_\phi}{\partial \rho} = - \frac{1}{\mu_o \sigma} \frac{\partial^2 B_z}{\partial \rho^2} \tag{16}$$

When Equations (15) and (16) are substituted into Equation (13), this yields

$$\frac{-1}{\mu_o \sigma} \frac{\partial^2 B_z}{\partial \rho^2} - \frac{1}{\rho} \frac{1}{\mu_o \sigma} \frac{\partial B_z}{\partial \rho} + i\omega B_z = 0 \tag{17}$$

or finally

$$\rho^2 \frac{\partial^2 B_z}{\partial \rho^2} + \rho \frac{\partial B_z}{\partial \rho} - (i\omega\mu_o\sigma\rho^2) B_z = 0 \qquad (18)$$

This is recognized as a Bessel equation and is readily solved by making the following standard substitutions. Let

$$r = \rho\sqrt{\omega\mu_o\sigma}\, e^{i\pi/4} \qquad (19)$$

Then Equation (18) reduces to

$$r^2 \frac{\partial^2 B_z}{\partial r^2} + r \frac{\partial B_z}{\partial r} - r^2 B_z = 0 \qquad (20)$$

which has a solution of the form [7].

$$B_z = C_1 I_o(r) + C_2 K_o(r) \qquad (21)$$

where $I_o(r)$ and $K_o(r)$ are Modified Bessel Functions of zero order. The constants C_1 and C_2 are evaluated by noting that at $r = 0$, $B_z(0)$ is finite, hence $C_2 = 0$ and that at

$$r = a\sqrt{\omega\mu_o\sigma} \qquad B_z\,(a\sqrt{\omega u_o\sigma}) = B_a$$

thus

$$C_1 = \frac{1}{I_o\,(a\sqrt{\omega\mu_o\sigma}\, e^{i\pi/4})}$$

Thus Equation (21) becomes:

$$B_z(\rho) = B_a \frac{I_o\left(\rho\sqrt{\omega\mu_o\sigma}\ e^{i\pi/4}\right)}{I_o\left(a\sqrt{\omega\mu_o\sigma}\ e^{i\pi/4}\right)} \tag{22}$$

If we make the following substitutions

$$\nu = \rho\sqrt{\omega\mu_o\sigma} = \sqrt{2}\ \rho/\delta \tag{23}$$

$$x = a\sqrt{\omega\mu_o\sigma} = \sqrt{2}\ a/\delta \tag{24}$$

where $\delta = \sqrt{2/\omega\mu_o\sigma}$ is defined as the skin depth ratio and the plasma radius (a) is to be treated as a parameter. Then Equation (22) reduces to

$$B_z(\nu) = B_a \frac{I_o(\nu\ e^{i\pi/4})}{I_o(x\ e^{i\pi/4})} \tag{25}$$

The modified Bessel Functions which have complex arguments can be reduced to "Kelvin Functions" which have real arguments [7].

$$I_o(x\ e^{i\pi/4}) = \mathrm{ber}_o\ x + i\,\mathrm{bei}_o x \tag{26}$$

$$I_o(\nu\ e^{i\pi/4}) = \mathrm{ber}_o\ \nu + i\,\mathrm{bei}_o \nu \tag{27}$$

Thus from Equations (13), (26) and (27), the time varying

magnetic field is written:

$$B_z(\nu,t) = B_a \frac{(\mathrm{ber}_o\nu + i\,\mathrm{bei}_o\nu)}{(\mathrm{ber}_o x + i\,\mathrm{bei}_o x)} e^{i\omega t} \tag{28}$$

Since only the real part of Equation (28) has any physical significance, Equation (28) becomes

$$\vec{B}_z(\nu,t) = \hat{i}_z B_a \frac{(\mathrm{ber}_o^2\nu + \mathrm{bei}_o^2\nu)^{1/2}}{(\mathrm{ber}_o^2 x + \mathrm{bei}_o^2 x)^{1/2}} \cos(\omega t + \theta_1) \tag{29}$$

where

$$\theta_1 = \tan^{-1} \frac{\mathrm{bei}_o\nu\ \mathrm{ber}_o x - \mathrm{ber}_o\nu\ \mathrm{bei}_o x}{\mathrm{ber}_o\nu\ \mathrm{ber}_o x + \mathrm{bei}_o\nu\ \mathrm{bei}_o x} \tag{30}$$

The equation for the electric field is obtained from the magnetic field by performing the derivative indicated in Equation (15)

$$\vec{E}(\nu,t) = \hat{i}_\phi \frac{\omega\delta}{\sqrt{2}} B_a \frac{(\mathrm{ber}_1^2\nu + \mathrm{bei}_1^2\nu)^{1/2}}{(\mathrm{ber}_o^2 x + \mathrm{bei}_o^2 x)^{1/2}} \cos(\omega t + \theta_2) \tag{31}$$

where

$$\theta_2 = \tan^{-1} \frac{\mathrm{bei}_1\nu\ \mathrm{ber}_o x - \mathrm{ber}_1\nu\ \mathrm{bei}_o x}{\mathrm{ber}_1\nu\ \mathrm{ber}_o x + \mathrm{bei}_1\nu\ \mathrm{bei}_o x} \tag{32}$$

The expression for the power distribution within the plasma

can now be developed with the use of Equation (31). From Poynting's theorem we have the power transferred to the plasma

$$P = \sigma \int_{-\ell/2}^{\ell/2} \int_{0}^{2\pi} \int_{0}^{x} E^2 \, \rho d\rho \, d\phi \, dz \tag{33}$$

for the case considered here, Equation (33) becomes

$$P = \frac{2\pi\ell\sigma\omega^2\delta^4 B_a^2}{4} \int_{0}^{x} \frac{(ber_1^2\nu + bei_1^2\nu)\nu d\nu}{(ber_o^2 x + bei_o^2 x)} \tag{34}$$

upon integration this reduces to

$$P = \frac{2\pi\ell\omega a^2}{\mu_o} B_a^2 \frac{1}{x} \left\{ \frac{ber_1 x \, (ber_o x - bei_o x)}{(ber_o^2 x + bei_o^2 x)} + \frac{bei_1 x \, (ber_o x + bei_o x)}{(ber_o^2 x + bei_o^2 x)} \right\} \tag{35}$$

Equation (35) gives the power in the plasma in terms of the discharge geometry, the applied magnetic field, and the plasma radius to skin depth ratio $x = \sqrt{2}\, a/\delta$.

II. PLASMA RADIUS TO SKIN DEPTH RATIO

We want to plot plasma power as a function of $x = \sqrt{2}\, a/\delta$ because we are interested in the variation of plasma power with plasma radius and skin depth. This is accomplished by making the following substitution

$$P_o = \frac{2\pi \ell \omega a^2}{\mu_o} B_a^2 \tag{36}$$

Thus Equation (35) can be written as

$$\frac{P}{P_o} = \frac{1}{x}\left[\frac{ber_1 x\,(ber_o x - bei_o x)}{(ber_o^2 x + bei_o^2 x)} + \frac{bei_1 x\,(ber_o x + bei_o x)}{(ber_o^2 x + bei_o^2 x)}\right] \tag{37}$$

This ratio, P/P_o, the ratio of the power in the plasma to the input power is plotted in Figure 2. Note that the maximum value of the ratio occurs at $x = \sqrt{2}\ a/\delta \cong 2.5$. This can be interpreted as the condition for an impedance match between the primary and secondary of a transformer; hence, the condition for maximum operational efficiency of the discharge is

$$a\sqrt{\sigma \mu_o \omega} = 2.5 \tag{38}$$

Although this is the optimum point of operation, this condition alone is not sufficient to determine the size of the discharge.

III. POWER MEASUREMENT

As Eckert points out [4], the most important experimental parameter to report for correlation between different experimenters is the magnetic field B_a. As it is shown in Equation (36), the input power to the plasma is determined

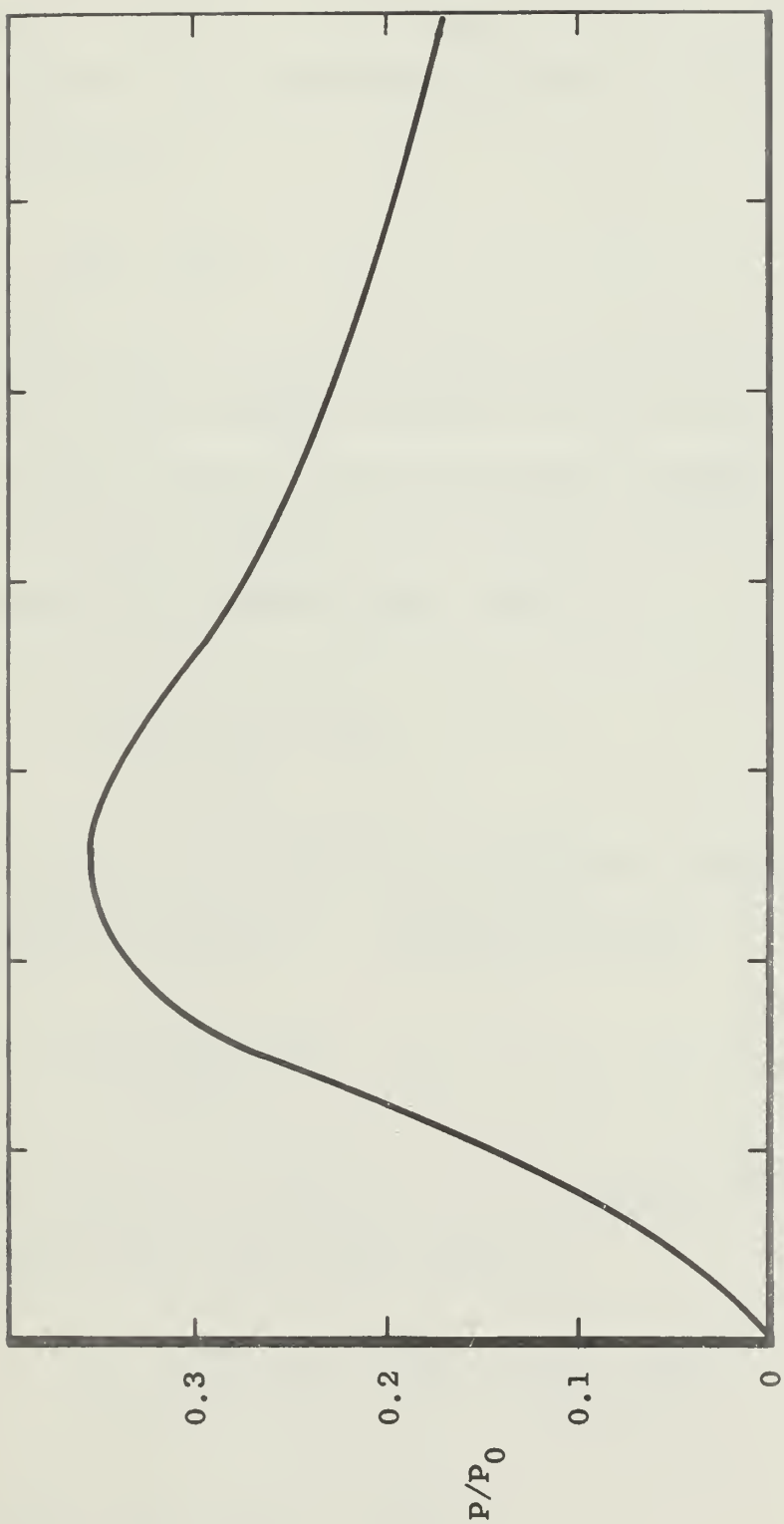

Figure 2. Power versus Plasma Diameter.

by B_a. B_a was measured using the rf current-transformer shown in Figure 3. The magnetic field B_a for a coil with n turns per unit length whose length is long compared to its radius is

$$B_a = \mu_o nI \tag{39}$$

The RMS current I_L can be obtained using the rf transformer on the straight portion of the lead from the coil to the oscillator. The relationship between the current in a straight wire and the magnetic field can be obtained directly from Ampere's Law. That is

$$I = \frac{1}{\mu_o} \oint_C \vec{B} \cdot \vec{d\ell} \tag{40}$$

The geometry for the field and line of integration C is shown in Figure 3. Integration gives

$$\vec{B} = \frac{\mu_o I}{2\pi\rho} \hat{\imath}_\phi e^{i\omega t} \tag{41}$$

From Faraday's induction law, the induced EMF of a loop through which this field passes is

$$V_{ind} = \frac{d}{dt} \iint \vec{B} \cdot \hat{n} dS = \iint \frac{\partial \vec{B}}{\partial t} \cdot \hat{n} dS \tag{42}$$

For the loop shown in Figure 3

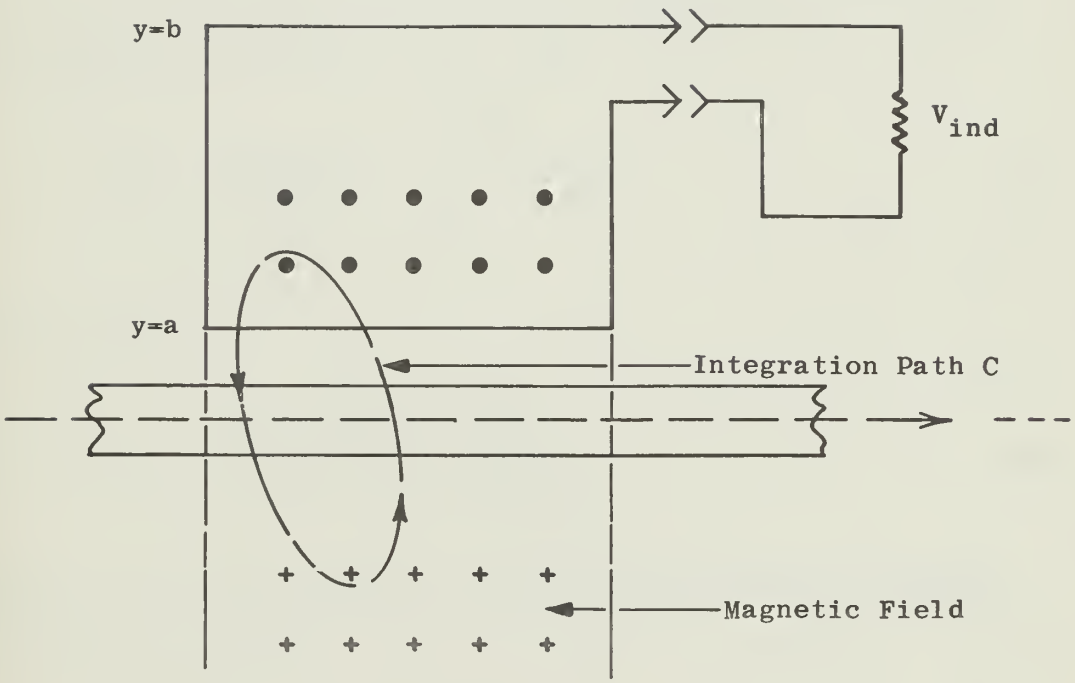

Figure 3. Diagram of Radio Frequency Current Transformer.

$$\hat{n} = \hat{i}_{\phi}$$

and

$$\hat{n} \cdot \frac{\partial \vec{B}}{\partial t} = \frac{i\omega t \mu_o I\, e^{i\omega t}}{2\pi\rho} \tag{43}$$

Thus the induced voltage in a loop normal to a straight wire carrying a current $I\, e^{i\omega t}$ is

$$v(t) = \frac{\omega \mu_o I\, e^{i\omega t}}{2\pi} \int_0^{\ell} \int_{y_a}^{y_b} \frac{d\rho}{\rho}\, dz \tag{44}$$

which yields

$$v(t) = \frac{\omega \mu_o I\, e^{i\omega t}}{2\pi}\, \ell \ln\left(\frac{y_b}{y_a}\right) \tag{45}$$

Since we are interested in the RMS value of the induced voltage V_{ind}, then

$$(V_{ind})^2 = \frac{1}{T} \int_0^T v(t)^2 dt \tag{46}$$

where $T = \frac{2\pi}{\omega}$, the period. Then

$$V_{ind} = \frac{\omega \mu_o \ell \ln \frac{y_b}{y_a}\, I_L}{2\pi} \tag{47}$$

where I_L is the RMS value of the current in the load coil. Solving Equation (47) for I_L and substituting into Equation (39) gives

$$B_a = \frac{2\pi n}{\omega \ell \ln \left(\frac{y_b}{y_a}\right)} V_{ind} \tag{48}$$

When Equation (46) is substituted into Equation (34), we obtain the input power into the plasma as a function of the induced voltage V_{ind} and the associated discharge geometry.

$$P_o = \frac{8\pi^2 n^2 a^2}{\ell \mu_o \omega} (V_{ind})^2 \tag{49}$$

The input power to the plasma may also be measured by using the voltage developed across the oscillator resonate circuit V and the total rf grid current I_T, as illustrated in Figure 4. Since the oscillator circuit is at resonance, the resonant circuit and the plasma appear as a resistance to the rf generator. Hence, under these conditions the rf input power into the plasma is

$$P_1 = I_T V \tag{50}$$

It should be noted that due to the high Q of the work coil, essentially all of the power P_o is actually delivered to the plasma.

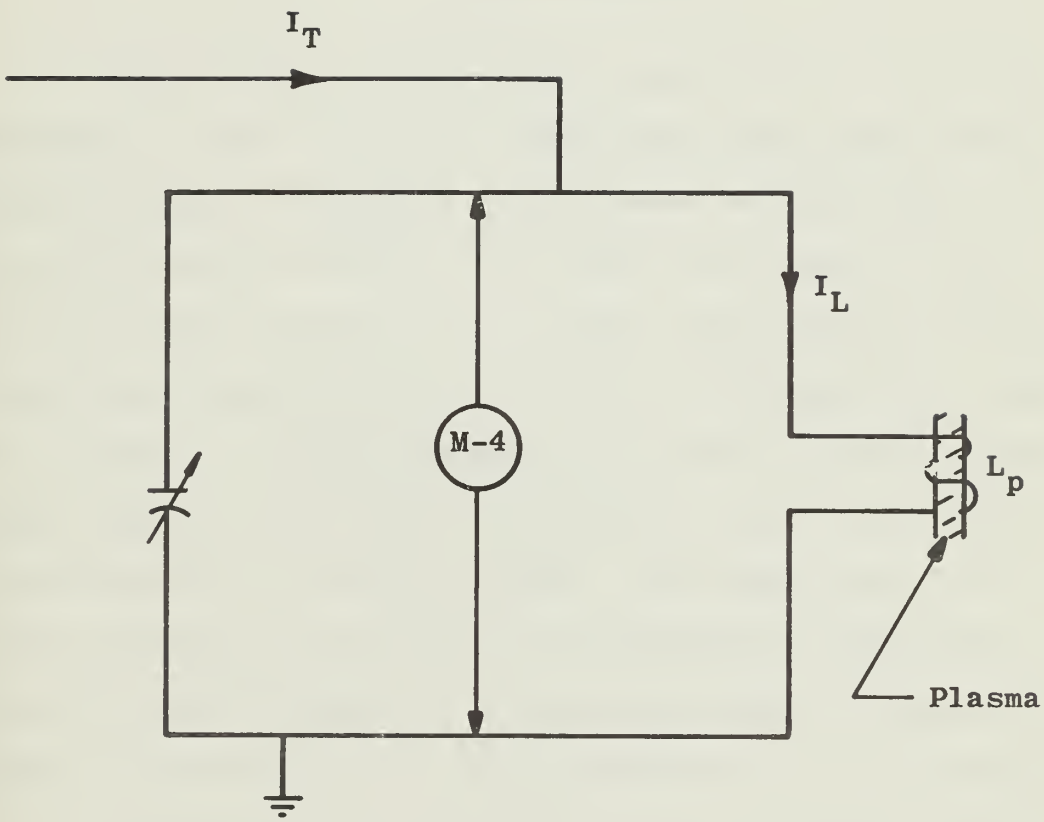

Figure 4. Equivalent Resonance Circuit.

CHAPTER III

EXPERIMENT

I. PLASMA DEVICE

The cylindrical plasma was contained in a 4.5 inch diameter, 9 inch long quartz tube which was mounted vertically as shown in Figure 5. The closed end was fitted to facilitate water cooling of the cover plate and to introduce the argon through four 1/8 inch copper tubes axially directed and symmetrically placed in the quartz tube. There are 20 holes, .035 inch diameter, drilled in each 1/8 inch copper tube and the tubes are aligned so that the initial flow direction is radially inward. The other end of the quartz chamber was connected to a mechanical vacuum pump which was used to pump the plasma device down to approximately .55 mm Hg prior to each initiation of the discharge.

The quartz tube and the end cover plate were separated from the remaining portion of the plasma device by an O-ring seal. This provided a good vacuum seal when operating at low pressures. The O-ring seal also provided electrical insulation so that the discharge was electrically floating. Additional electrical isolation of the plasma was obtained by placing a one inch section of plexiglass between the flanged mounting brackets of the existing section of the plasma device and the lower portion of the quartz tube.

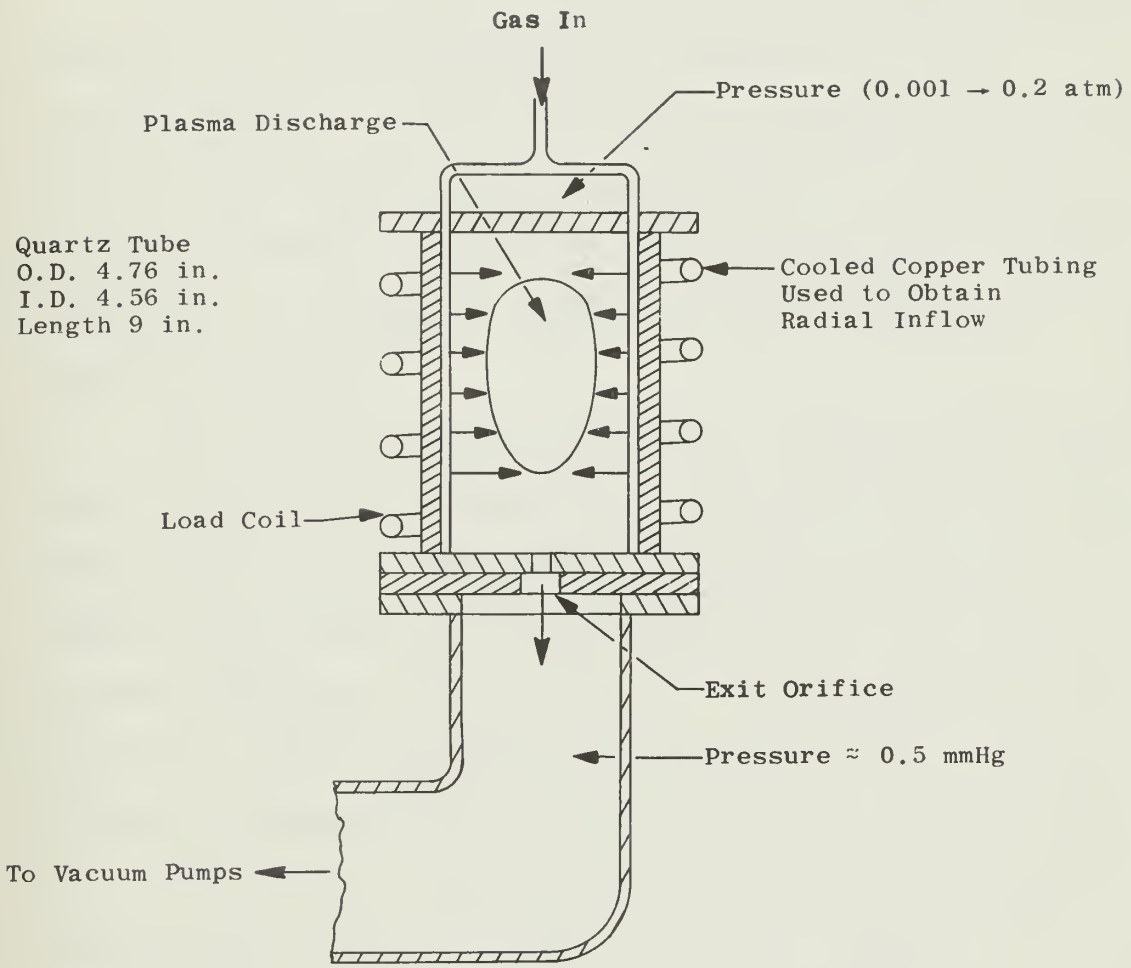

Figure 5. Plasma Device.

II. OSCILLATOR

The oscillator which provided the rf power for the production of the electrodeless discharge is of the Colpitts design. Among the variety of possible oscillator designs, the Colpitts was chosen because of its exceptionally good frequency stability under widely varing loaded conditions. A schematic diagram of the oscillator is shown in Figure 6.

The heart of the oscillator is a water cooled high power triode which is capable of delivering up to 50 kilowatts of rf power. The tuning capacitors C_p and C_g are remote controlled motor driven capacitors. C_p is used as a coarse adjustment and C_g is for fine adjustments of the oscillator. The load coil of the oscillator L_p is wound around the quartz tube in which the plasma is generated.

The load coil was constructed of 1/4 inch copper tubing water cooled for safety purposes. However, the water was not turned on for a few runs, and no noticeable heating was observed. This shows that very little power is dissipated in the work coil. To prevent arcing between the coil and the metal cabinet containing the oscillator, the copper tubing was fed out of the oscillator through a one inch plexiglass plate as shown in Figure 7.

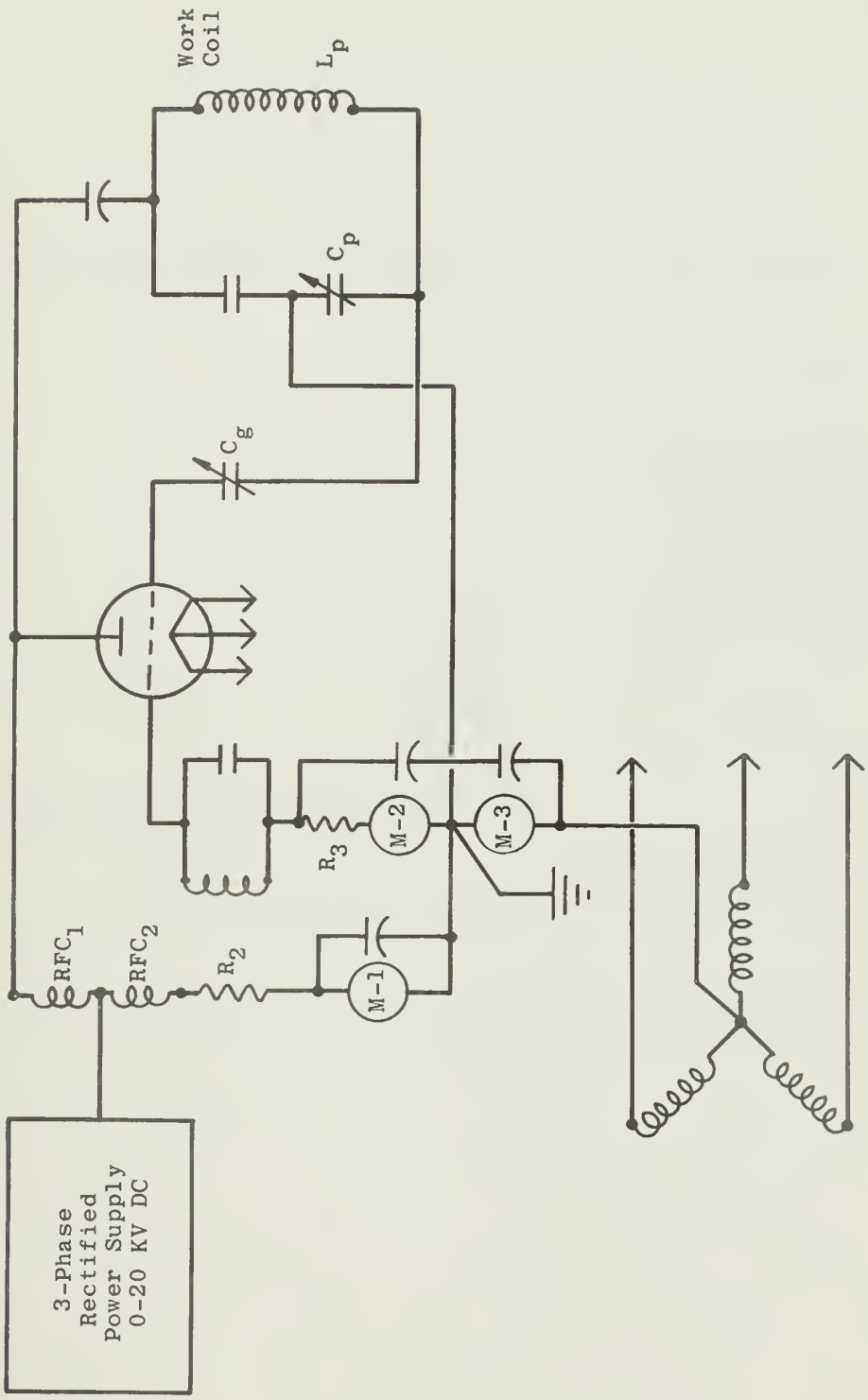

Figure 6. Radio Frequency Oscillator Schematic.

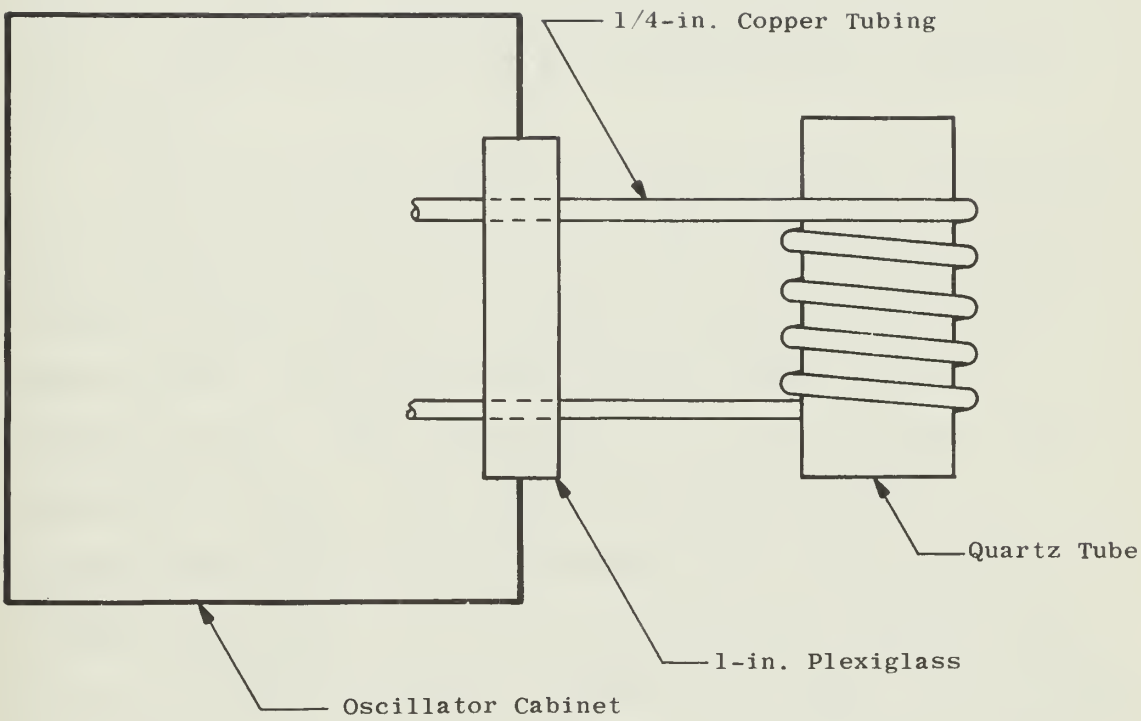

Figure 7. Copper Tubing Exit and Plasma.

III. OPERATING CHARACTERISTICS

To produce the discharge, the test cell is pumped down to approximately .001 atmospheres. The argon regulator valve is set for the line pressure to be in the neighborhood of 150 psi. Before igniting the plasma, it is best to purge the system by bleeding some argon through the system.

The oscillator resonant circuit is tuned by varying C_g to obtain a clean sine wave on the oscilloscope with a maximum voltage output. A pleasantly pink glow should appear within the quartz tube when the oscillator is properly tuned. This discharge is of the low-power type described earlier. The oscillator plate voltage is increased from 2 KV to approximately 10 KV. As the plate voltage increases, the dc grid current will increase from 50 ma to as much as 800 ma. During this time, the discharge will change from pink to pink-red, then to a yellow-white color. At the same time, the plasma is contracting away from the end corner plates of the quartz tube and continues to contract until the plasma is confined entirely within the load coil. The discharge at this point changes from the low-power to the high-power discharge. If there are any leaks in the system; that is, if air is mixed with the argon, the system will be very difficult to ignite in the high-power mode.

Once the discharge is in the high-power mode, the gas flow and power are increased simultaneously. Prior to increasing the gas flow, the discharge has been attached to the wall of the quartz tube. The radial inflow of the argon tends to "blow" the discharge away from the walls. The final stable configuration of the plasma is obtained by careful adjustment of the flow rate and power input which result in a "hot plasmoid" as illustrated in the photographs presented in Figure 1, page 4.

Typical plasma operating conditions are as follows:

(1) DC plate voltage . . . . . 8 KV.

(2) DC current . . . . . 1.6 amps.

(3) DC grid current . . . . . .050 amps.

(4) Chamber pressure . . . . . 1 atmos.

(5) Flow rate . . . . . 5×10^{-4} lbs/sec.

At one atmosphere of pressure and with increased gas flow, the discharge becomes much more intense, and vacillates within the discharge without touching the wall. The vacillating plasma can be stabilized by the proper adjustment of input power and gas flow rate. In addition, the stability of the discharge is strongly dependent on the manner in which the flow is introduced. For example, the discharge is quickly "blown out" unless the increase in gas flow rate is accompanied by a corresponding increase in input power.

Reed [8] reports that the most stable operation is obtained with a tangential flow of the argon, which causes the gas to spiral down the walls. This tends to create a low-pressure region in the center of the tube, which causes some of the plasma to flow upstream countercurrent to the main flow. Contrary to Reed's report, it is found in this experiment that tangential inflow tended to "blow out" or extinguish the discharge unless enormous amounts of input power were dumped into the plasma.

The most stable plasma for any given power or gas flow rate was found to exist with a radial inflow of argon. With radial inflow, the plasma filled the volume within the solenoid except for a small region near the walls and vacillation was not observed. Radial inflow yields the optimum stability when input power, gas flow rate, conductive and radiative power are considered. This is in agreement with recent theoretical study by Keefer [3] who predicts improved stability with radial inflow.

IV. INSTRUMENTATION

The instrumentation required to monitor the electrodeless discharge can be divided into two different categories:

(1) Those required to monitor gas dynamic effects; for example, instrumentation for mass flow rates, chamber pressure and line pressures.

(2) The electrical instrumentation used to monitor the rf energy; for example, the high voltage rf and dc voltmeters, ammeters, and specially designed instruments for particular plasma measurements.

The gas dynamic system is illustrated in Figure 8 and a diagram of the electrical instrumentation layout is shown in Figure 9. The primary instruments for monitoring the oscillator consist of: M-1, the dc plate voltage of the oscillator tube; M-2, the dc grid current; and M-3, the dc cathode current. M-1, 2, and 3 provided the total dc power into the system. A detailed account of power calculations are presented in the theory section of this work.

One of the most important parameters of the plasma is the current through the load coil, since this current along with geometry of the coil can be used to correlate data between different investigations. The load coil current was measured using the rf current-transformer measuring device T-1 designed by the author and shown in Figure 10. The rf transformer was fabricated from a one inch slab of plexiglass, and mounted on the copper feed-in line to L_p. The copper tubing was wrapped with three or four turns of teflon tape to prevent arcing between the transformer windings and the copper line. The EMF generated in T-1 was fed out through a shielded coaxial cable to the 434 Hewlett-Packard voltmeter.

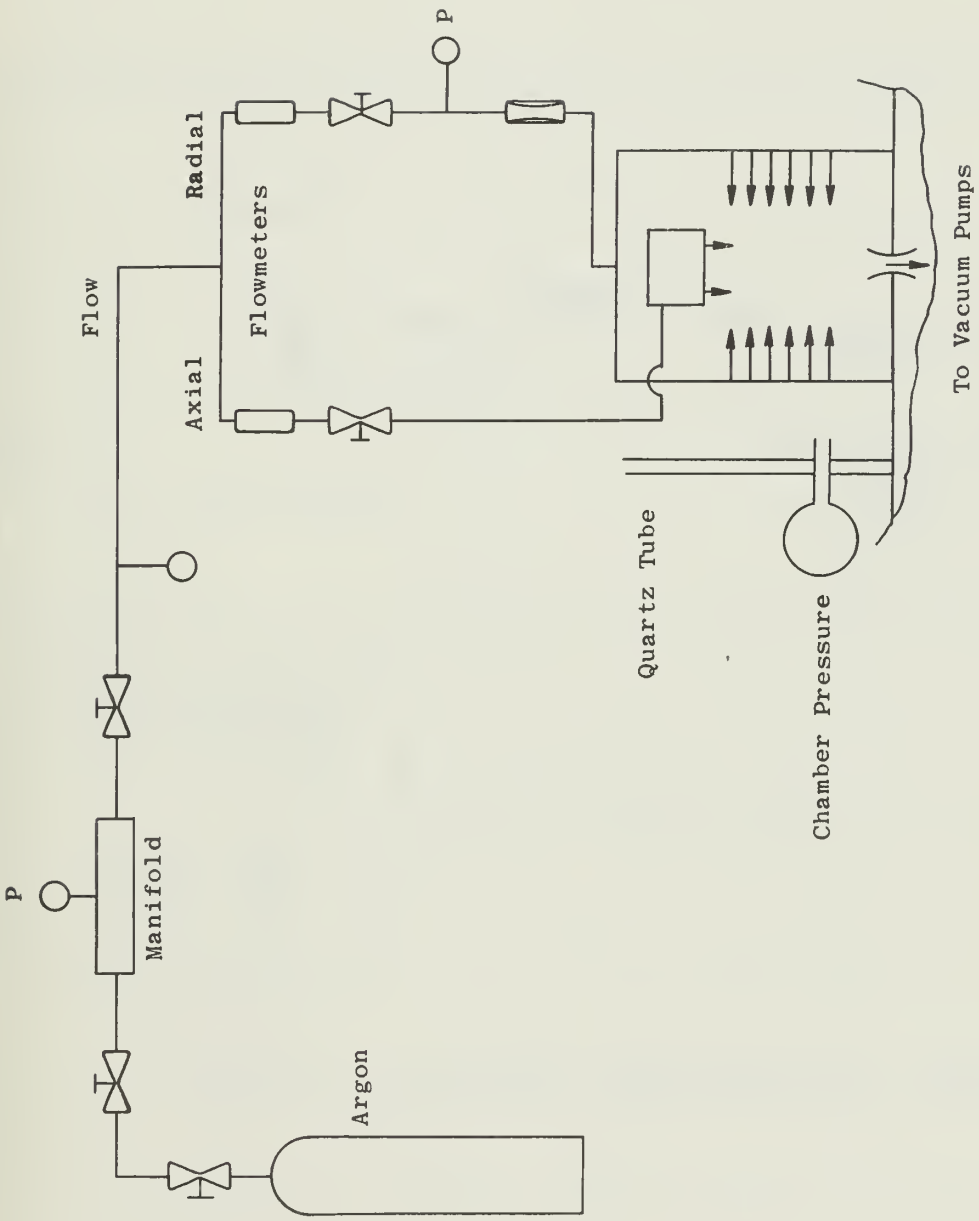

Figure 8. Gas Flow Diagram.

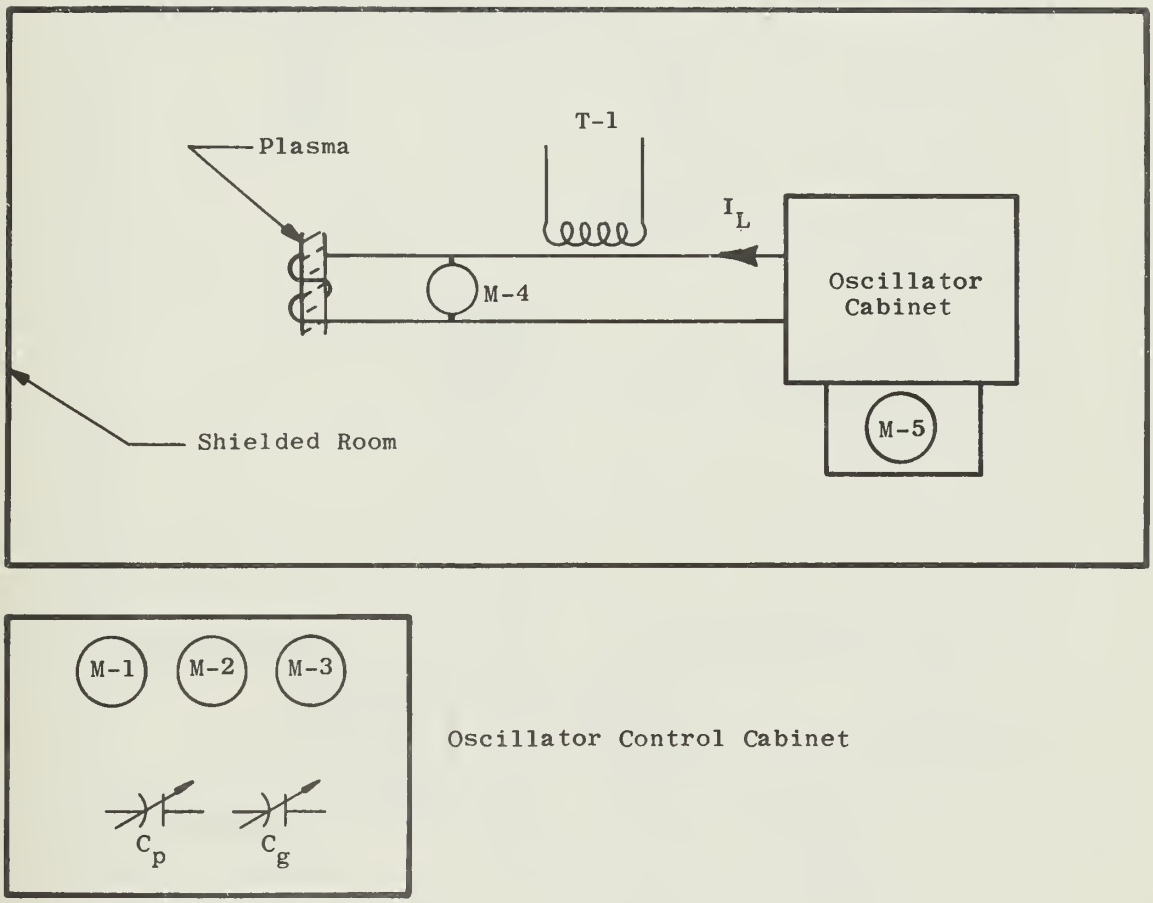

Figure 9. Electrical Instrumentation Layout.

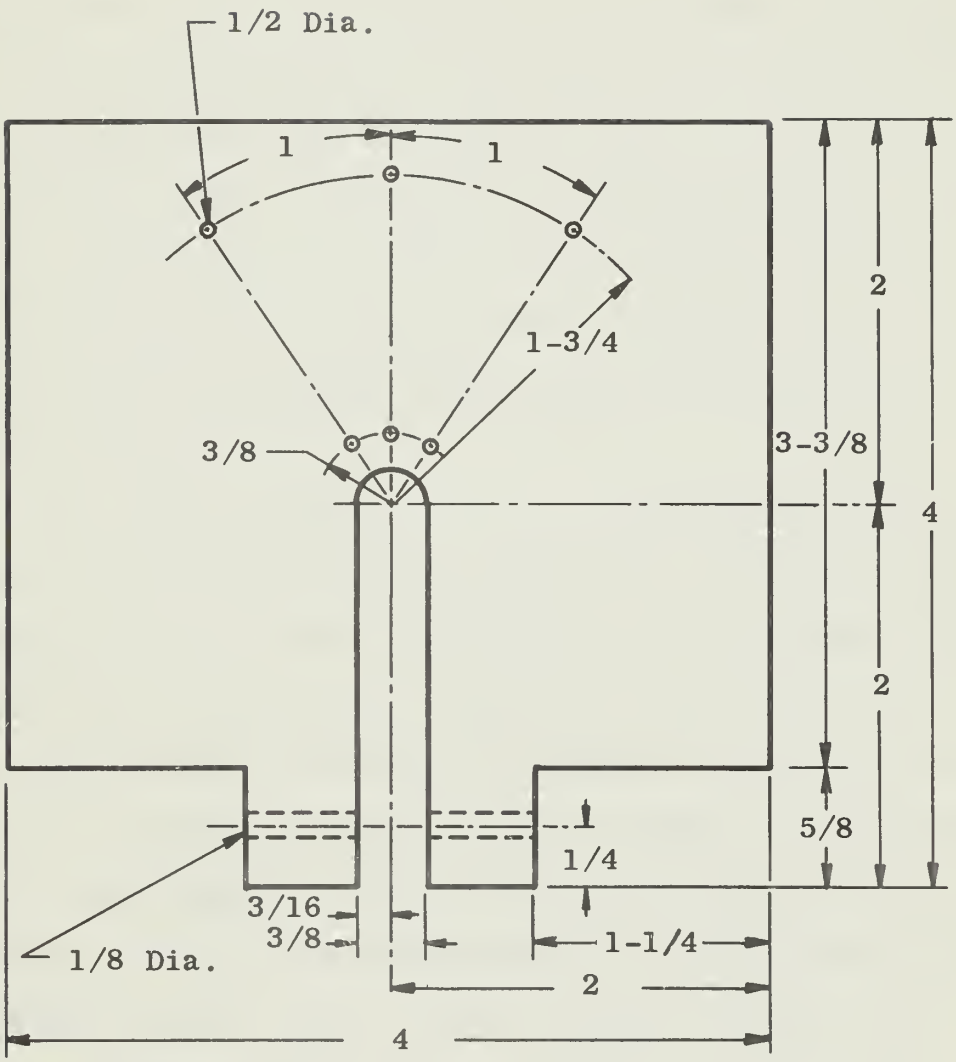

All Dimensions in Inches

Figure 10. Radio Frequency Current Transformer Measuring Device.

A high voltage vacuum tube voltmeter, M-4, was designed by the author to measure the rf voltage across L_p. Due to the extremely high voltage and the rf frequencies involved, the meter was designed to float electrically in the circuit. This was achieved by mounting the tube, components, and meter in a light aluminum chasis which was hung across L_p with a pair of sturdy alligator clips. A diagram showing the meter mounting and the circuitory is shown in Figure 11.

The total rf line current I_T was measured with a Hewlett-Packard 456 rf current probe M-5. To insure proper readings, the meter case was attached to the cabinet containing the rf oscillator. Since the total RMS value of the rf grid current exceeded the maximum current of the probe, the oscillator grid line was divided into four equal paths. The measured value was then multiplied by four. The output of the rf current probe M-5 was fed out through a shielded coaxial cable mounted inside a copper tube. The copper feed-out line was grounded to the rf shield enclosing the room and the oscillator cabinet. This insured that the meter was at rf ground.

The oscillator frequency was monitored using an rf frequency meter and a standard oscilloscope. A schematic diagram of the electronic instrumentation is shown in Figure 12.

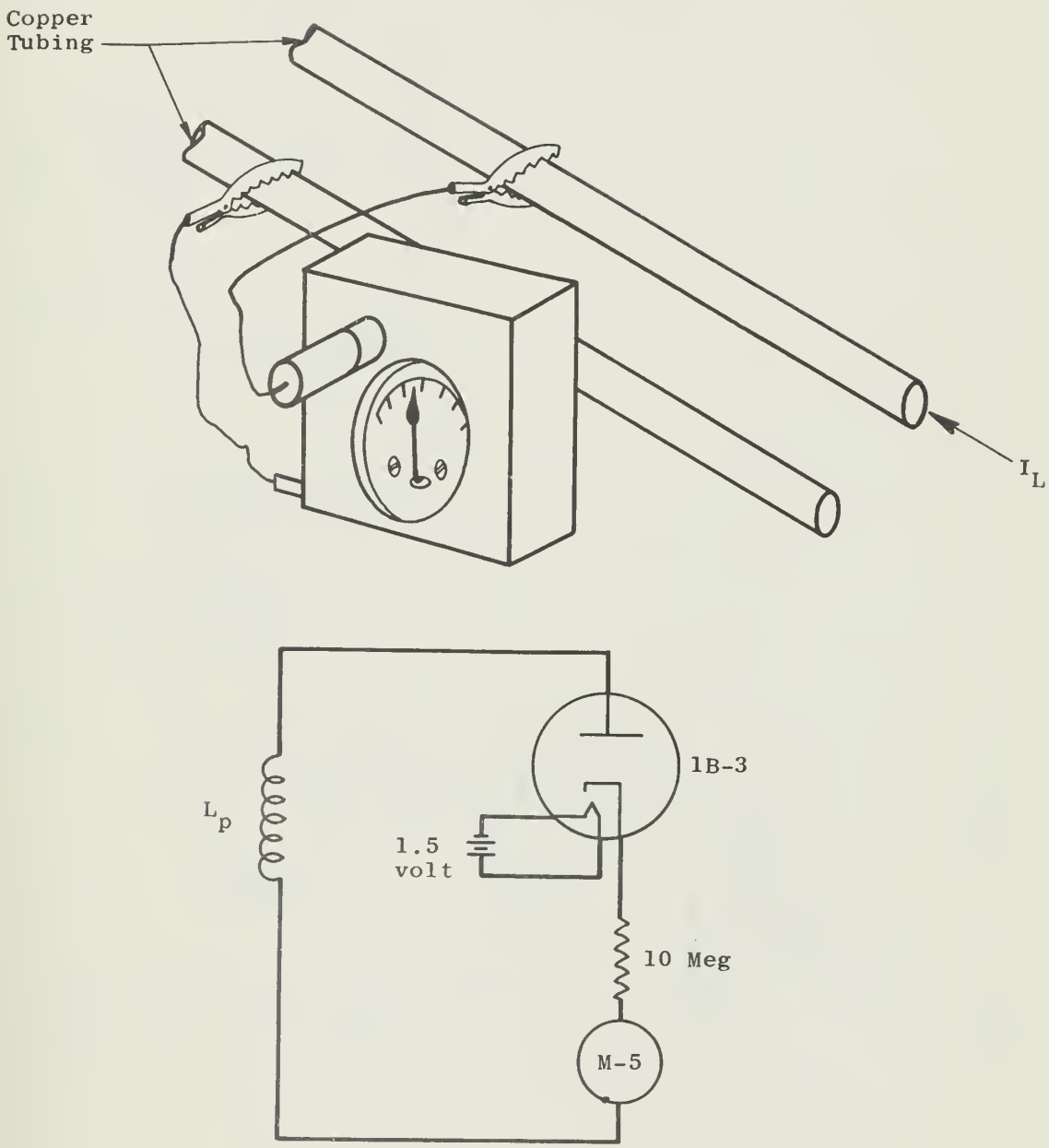

Figure 11. High Voltage Meter Mounting and Circuit Schematic.

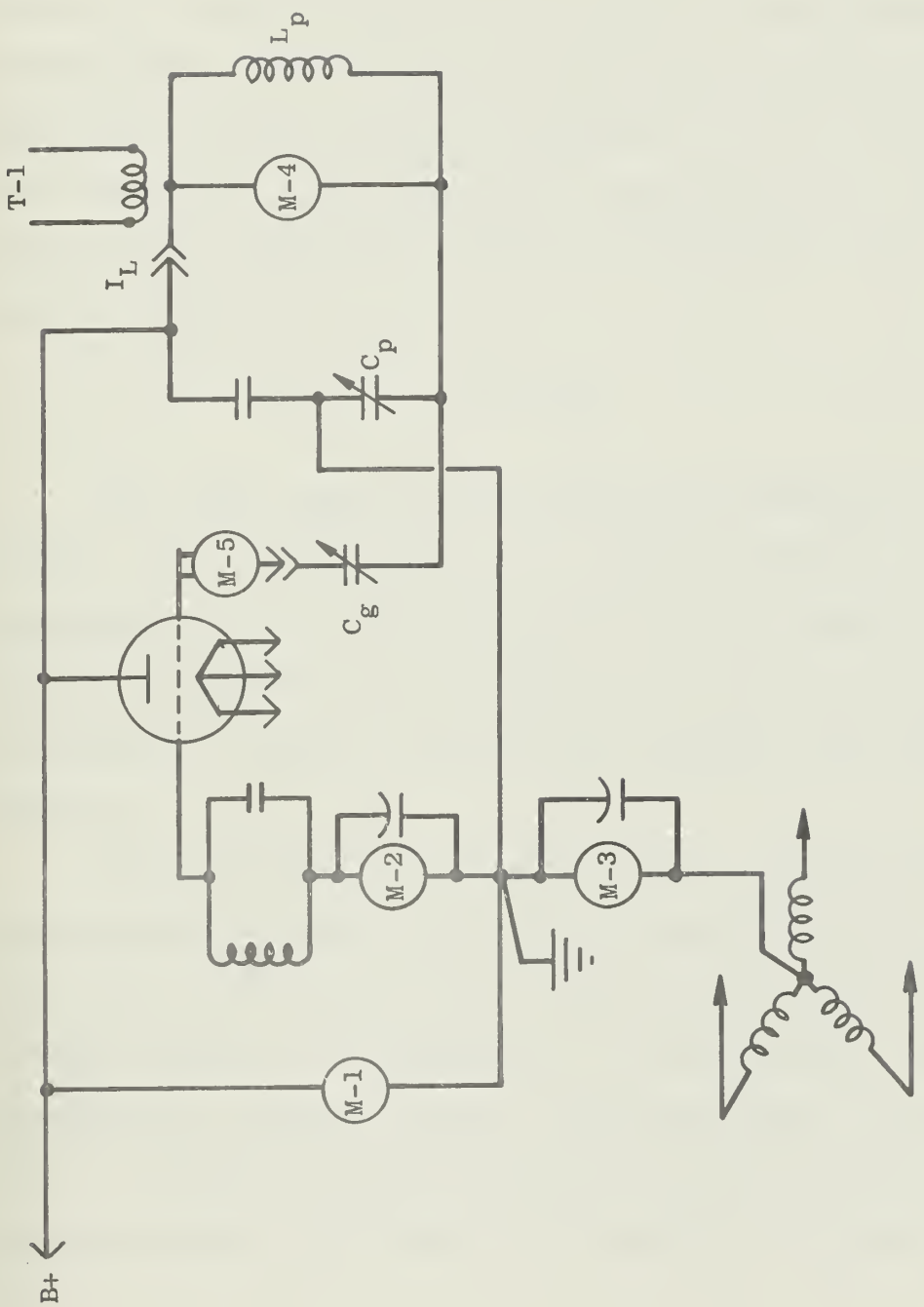

Figure 12. Electrical Instrumentation Schematic.

As a final note concerning the electrical instrumentation, it should be pointed out that each measurement was obtained only after tediously eliminating parasitic oscillations which seemed to exist everywhere in the vicinity of the rf generator. All electrical instrumentation near the generator was eventually placed at rf ground by the "cut and try" method.

IV. DATA

The input power to the plasma was measured by two methods, with the generator in a stable condition; i.e., the plasma was not vacillating and was not touching the wall of the quartz tube and operating at one atmosphere of pressure. The gas flow was held constant throughout the runs.

The oscillator dc cathode current and plate voltage were measured to obtain the total dc power into the system. Then, while monitoring the dc instrumentation the induced voltage from the rf transformer T-1 was recorded. After recording the induced voltage, the meter output was checked with T-1 removed from the circuit to ensure that the recorded value was not riding on an unwanted rf ground potential.

Next, the total rf grid current, I_T, was measured by connecting the output load of the rf probe to the 434 Hewlett-Packard voltmeter. Again, as in the previous

measurement, the circuit was checked for unwanted rf ground potentials. After recording the induced voltage (B_a) and the total rf grid current, I_T, the dc power level was changed and the procedure repeated. Three different dc power settings were used.

The oscillator efficiency is determined as

$$\frac{P_o}{P_{dc}} \times 100 = \text{efficiency} \tag{51}$$

The efficiency of the oscillator was found to be 77 percent. This is a typical value for a class "C" operated high power oscillator. An oscillator efficiency of 81 percent is reported by Dresvin, Donskoi, and Gol´dfarb [6] using calorimetric and spectroscopic techniques on an argon electrodeless discharge operated at one atmosphere.

The results of the power measurements and the oscillator efficiency calculations for the three power settings are presented in Tables I through IV. Table I gives the results as predicted using Thomson's theory, Equation (49), and Table II gives the results obtained from the resonant circuit current and voltage measurements, Equation (50).

The measured value of $\sqrt{2}\ a/\delta$ ranged from 14.4 with a = 2.26 inch (at the wall) to 12.2 with a = 2.00 inch. These values of $\sqrt{2}\ a/\delta$ were obtained by measuring the diameter of the high-power plasma discharge from photographs

TABLE I

POWER MEASUREMENTS FROM THOMSON'S THEORY

Induced[a] Voltage (volts)	Load Coil Current (amps)	Magnetic Field ($Weber/m^2$)	Normalized[b] Power (watts)
24	66.0	3.32×10^{-4}	4,610
25	68.5	3.53×10^{-4}	5,000
26	71.5	3.63×10^{-4}	5,500

[a] $\pm$ .5 Volts

[b] $\pm$ 200 Watts

TABLE II

POWER MEASUREMENTS FROM CIRCUIT VOLTAGE AND CURRENT

Total[a] Current (amps)	Coil[b] Voltage (volts)	Radio Frequency[c] Power (watts)
1.8	2,500	4,550
1.9	2,500	4,900
2.1	2,500	5,250

[a] ± .04 Amperes

[b] ± 50 Volts

[c] ± 340 Watts

TABLE III

OSCILLATOR EFFICIENCY

Cathode[a] Current (amps)	Plate[b] Voltage (volts)	DC[c] Power (watts)	Normalized Power (watts)	Efficiency (percentage)
1.25	4,800	6,000	4,600	77
1.3	5,000	6,500	5,000	77
1.4	5,100	7,150	5,500	77

[a] ± .02 Amperes

[b] ± 150 Volts

[c] ± 310 Watts

TABLE IV

COMPARISON OF THOMSON MODEL WITH CIRCUIT CURRENT AND VOLTAGE MEASUREMENTS

DC Power (watts)	Plasma Input Power (watts)	Radio Frequency Power (watts)
6,000	680	4,550
6,500	735	4,900
7,150	790	5,250

of the runs and from conductivity values obtained from Knopp [9]. A value of plasma temperature of 9,000°K, [10] was used to obtain the conductivity value of 2,000 mhos/m from the data presented [9]. Using the average conductivity of 2,000 mhos/m [6] obtained from spectroscopic measurements on a similarly operated argon discharge, the value of $\sqrt{2}\ a/\delta$ ranged from 17.2 with (a) at the wall to 15.3 with a = 2.00 inch. Thus, the plasma device is operating somewhat below its maximum possible state. This is in disagreement with the position of Hollister [1] who states that the plasma will always adjust itself to a value of $\sqrt{2}\ a/\delta \approx 2.5$. For the plasma to adjust to $\sqrt{2}\ a/\delta = 2.5$, with a = 2.00 inch, the value of the electrical conductivity needed would be on the order of 20,000 mhos/m. The measured values of $\sqrt{2}\ a/\delta$ are in agreement with Keefer's theory [3] and Sprouse's results [10]. Both state that the plasma is wall dominated.

CHAPTER IV

DISCUSSION OF RESULTS

As can be seen from Table IV, page 40, the power predicted by the Thomson model as determined by Equation (35) is much less than the rf power available to the plasma determined by Equation (50) from measurements of circuit current and voltage. The cause of this difference is not understood. The assumptions of the Thomson model may not be adequate for the complex problem of rf plasma discharges. For example, the consequences of neglecting end effects and of assuming the conductivity to be constant both radially and longitudinally are not known. The field calculations of the Thomson model in Equation (35) depend upon a uniform slab of conductive material within a uniform magnetic field, where as the conductivity of the rf gaseous discharge varies with both the radial and axial coordinates [6] and the uniformity of the magnetic field within the plasma is not known. Furthermore, the calculation of power by Equation (35) requires the measurement of the induced voltage from which B_a and consequently P_o are determined. The measurement of the induced voltage used to determine B_a could have introduced an unknown and perhaps large error, since only a one volt variation can cause a difference of several

hundred watts of output power, see Table I, page 37. The transformer T-1 used in measuring B_a was not calibrated because there were no means available for the calibration on the present experiment. However, great care was taken to shield the cable thereby minimizing any induced ground potentials.

The fault may not all be with the Thomson model. These results open to question the validity of accepting determinations of rf power by measuring the circuit current and voltage as being the power that actually goes into the plasma. It would appear that further investigation is needed to resolve the issue.

The meter movements used to measure the currents and voltages in Tables I, II, and III, pages 37, 38, and 39, were accurate to one percent of the full scale reading. The limits of accuracy as indicated in the table footnotes were determined by the delta method.

CHAPTER V

CONCLUSION

In conclusion, the input power to the plasma was measured by two methods: one based on the Thomson model, and the other on the circuit current and voltage measurement. There was a marked difference between the results of the two methods. The reason for this difference is not fully understood, although several possible weaknesses of each method are put forth and discussed. It is believed that further theoretical and experimental study of the plasma power should be undertaken.

BIBLIOGRAPHY

BIBLIOGRAPHY

1. Hollister, D. D. "An Investigation of the High Pressure Electrodeless Arc in Air," Air Force Flight Dynamics Laboratory Report No. AFFDL-TR-68-160, Wright-Patterson Air Force Base, Ohio, February, 1969.

2. Babat, G. J. "Electrodeless Discharges and Some Allied Problems," Journal of the Institution of Electrical Engineering, (London) 94:27-37, February, 1947.

3. Keefer, R. D. "The Confined Electrodeless Arc." Paper presented at the American Physical Society Symposium on the Physics of High Pressure Arcs, Gatlinburg, Tennessee, October, 1969.

4. Eckert, H. U. "Analytical Solution of the Energy Balance Equation for Thermal Induction Plasmas in Argon." American Institute of Aeronautics and Astronautics Paper No. 68-711, AIAA Fluid and Plasma Dynamics Conference, Los Angeles, California, June, 1968.

5. Sprouse, J. A. "Coupling Mechanism Between RF Excited Coils and Conductive Media." American Institute of Aeronautics and Astronautics Paper No. 68-710, AIAA Fluid and Plasma Dynamics Conference, Los Angeles, California, June, 1968.

6. Dresvin, S. V., A. V. Donskoi, and V. M. Gol´dfarb. "Determination of the Conductivity of a High-Frequency Discharge in Argon by Calorimetric and Spectral Methods," Soviet Physics - Technical Physics, 10:1270-1274, March, 1966.

7. Abramowitz, M., and I. A. Stegun (editors). Handbook of Mathematical Functions. National Bureau of Standards, United States Department of Commerce. Washington: Government Printing Office, 1967.

8. Reed, T. B. "Induction - Coupled Plasma Torch," Journal of Applied Physics, 32:821-824, May, 1961.

9. Knopp, C. F., and A. Campbel. "Experimental Determination of the Thermal Conductivity of Atmospheric Argon Plasma," Physics of Fluids, 9:989-996,

10. Sprouse, J. A. Private communication. Arnold Engineering Development Center, Arnold Air Force Station, Tennessee, December, 1969.

APPENDIX

APPENDIX A

CYLINDRICAL COORDINATES

A diagram illustrating cylindrical coordinates used in the discharge is shown in Figure A-1. The curl of a vector $\vec{A}$ in cylindrical coordinates, is

$$\nabla \times \vec{A} = \frac{1}{\rho} \begin{vmatrix} \hat{i}_\rho & \rho\hat{i}_\phi & \hat{i}_z \\ \frac{\partial}{\partial\rho} & \frac{\partial}{\partial\phi} & \frac{\partial}{\partial z} \\ A_\rho & \rho A_\phi & A_z \end{vmatrix}$$

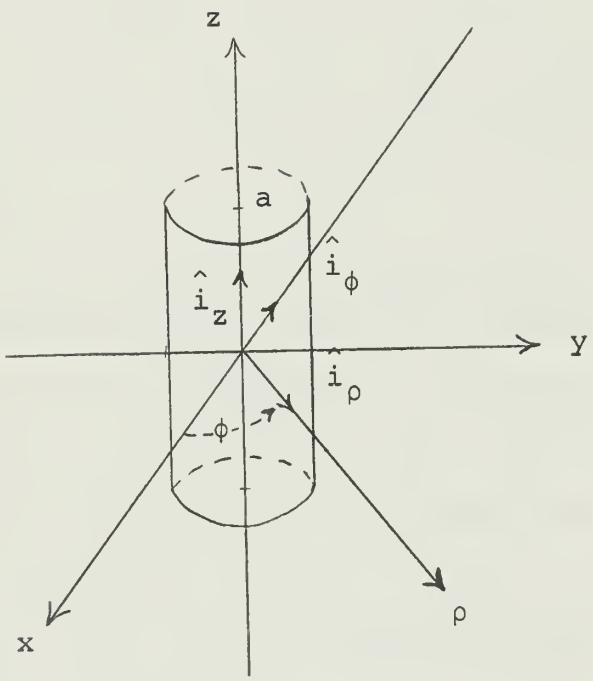

Figure A-1. Cylindrical Coordinates.

VITA

The author, William Lee Walker, was born on October 23, 1938, in Memphis, Tennessee. He attended Whitehaven High School in Memphis and completed high school through the U. S. Navy. Undergraduate work was started in September 1963 at the University of Hawaii and was completed at Memphis State University from which he was graduated in May 1968, with a major in physics. Financial assistance was provided through the Navy's Tuition Aid Program.

Graduate study was begun in January 1969, at The University of Tennessee Space Institute, Tullahoma, Tennessee, terminating in a Master of Science degree in March 1970. Graduate study was sponsored jointly through the U. S. Navy and a University of Tennessee scholarship.

The author has been a member of the U. S. Navy since October 1955, and holds the permanent rank of Chief Antisubmarine Warfare Technician.

He currently holds the rank of Lieutenant Junior Grade and is to be assigned to submarine duty. He is a member of the American Association of Physics Teachers and Sigma Pi Sigma National Physics HOnor Society.

Lt. and Mrs. Walker have four children, Steve 11, Theresa 9, Melba 8 and Garland 2.

Thesis
W22227 Walker
Determination of the imput power to a radio frequency electrodeless discharge.

117480